

Hirofumi TAKI · Toru SATO

High-resolution real-time three-dimensional acoustic imaging system with a reflector

Received: June 19, 2006 / Accepted: March 22, 2007

Abstract

Purpose. We propose an acoustic real-time three-dimensional (3-D) diagnostic imaging system based on a hybrid array–reflector configuration that realizes high time and spatial resolutions with a modest computational load.

Methods. All the elements on a small dense array were excited with proper time delays to transmit a broad beam similar to that of a single transmitter element. The echo was gathered by a concave reflector and received by the dense array. The image of the target was reconstructed by numerical back projection from the defocused image distributed on the array. With this scheme, images of the whole measurement area can be reconstructed from a single transmit and receive event.

Results. The number of elements can be reduced to about 1/8.2 that of a dense 2-D array of a digital beamforming system having the same spatial resolution. By weighting individual elements, the sidelobe level could be suppressed to less than -21 dB. The maximum theoretical frame rate is 5000 3-D images/s. This method has a higher signal-to-noise ratio than that of defocused multi-element digital beamforming methods, overcoming conventional phased array performance.

Conclusion. The proposed scheme is suited for purposes that require high time and spatial resolutions, such as cardiology.

Keywords ultrasound · hybrid method · synthetic aperture · phased array · real-time

Introduction

Volumetric three-dimensional (3-D) high-resolution acoustic images are in high demand for medical diagnoses. A

conventional phased-array imager excites all array elements to form a transmit beam, and it uses all of the elements for receive beamforming.¹ Although only the receive beam is dynamically focused, imaging under this condition results in a high electronic signal-to-noise ratio (SNR) as well as good spatial and contrast resolution. The main problem with such a configuration is that the number of elements becomes enormous for a 2-D array of a 3-D phased-array imager.

One strategy to reduce the cost and complexity of a 3-D phased-array imager is to use a linear or convex array that is moved mechanically.^{2–4} With such a method, the number of elements can be reduced greatly by using a 1-D array. The lateral resolution in the measurement plane is high because receive beams are focused dynamically. In the plane perpendicular to the longitudinal axis of the array, however, the transmit beam and the receive beam are focused on a fixed distance by acoustic lenses on the elements. Thus, the lateral resolution seriously deteriorates in front of and behind the focus. Moreover, this type of 3-D phased-array imager does not have satisfactory time resolution.

Another strategy to improve time resolution and decrease the number of elements, at the cost of some loss of lateral resolution and SNR, is to use a digital beamforming technique with a 2-D sparse array, with an element spacing of more than one-half of a wavelength.^{5–14} Such a method uses a wide transmit beam and multiple receive beams formed simultaneously. Although several array designs have been reported, it is difficult to reduce the number of elements to less than half that of the dense array.

Karaman et al.¹⁵ proposed that a single-element spatial response with high acoustic power could be synthesized by a defocused multi-element transmit subaperture. Lockwood et al.¹⁶ applied this scheme to a 3-D synthetic aperture imager with a 1-D array. Although the SNR was improved, lateral resolution deteriorated in the plane perpendicular to the array for the same reason as that of a phased-array imager with a 1-D array.

In this study, we propose a system based on a hybrid array–reflector configuration that realizes high time and

H. Taki (✉) · T. Sato
Department of Communications and Computer Engineering, Kyoto University, Yoshida-honmachi, Sakyo-ku, Kyoto 606-8501, Japan
Tel. +81-75-753-3366; Fax +81-75-753-3342
e-mail: taki@aso.cce.i.kyoto-u.ac.jp

spatial resolutions with modest computational load to resolve these problems. In this system, all elements on a small dense array are excited with appropriate time delays to synthesize a spatial response similar to that of a single element. The echoes from targets are first gathered by a concave reflector and then received by the array. The image of the target is reconstructed by numerical back projection¹⁷ from the defocused image distributed on the array.

In the following section, we first outline the framework of the proposed 3-D acoustic imaging system. We provide some necessary wave equations and parameters for evaluating the spatial resolution of this method. Then, we discuss optimization of the reflector shape and the array configuration for a wide measurement area with high spatial resolution. We propose a method to suppress the sidelobe level by employing a proper reflection coefficient of the mirror in the numerical back projection. The proposed method reconstructs images from received signals by numerical back projection; thus, the reflection ratio of the mirror can be set freely in the numerical back projection. We examine the spatial resolution of the proposed imager and compare the spatial resolution with that of current 3-D imagers. Furthermore, we evaluate improvements in the SNR with the proposed imager compared to conventional types, such as digital beamforming and phased-array imagers.

Materials and methods

Principle of the hybrid 3-D imaging system with a small dense array and a reflector

A digital beamforming imager transmits a wide beam to the whole measured area and receives echoes using a 2-D array. It then utilizes inverse Fourier transforms to form all the images in the measurement area. Since this imager makes a 3-D image from one transmit and receive event, it has high time resolution. However, a large 2-D array with an enormous number of elements is required to obtain high spatial resolution, which is thus very costly. We propose a system that decreases the number of elements but has the same high time and spatial resolutions.

Figure 1 shows a schematic of the acoustic real-time 3-D imaging system based on a hybrid array–reflector configuration. In this method, all elements on a small dense array are excited with proper time delays so that all transmit pulses are focused at a single point after reflecting from the mirror. The transmit pulses are then synthesized into a broad beam similar to that of a single transmit element with high acoustic power. The transmit beam is radiated over the entire measurement field from this focal point. The reflected echoes are first gathered by the concave reflector and are then received by the array, as shown in Fig. 2. Since the reflector and the array are fixed, a defocused image is distributed onto the array. The image of the target is reconstructed from the received signal on the array by numerical back projection.

Using this scheme, images of the whole area measured can be reconstructed from a single transmit and receive

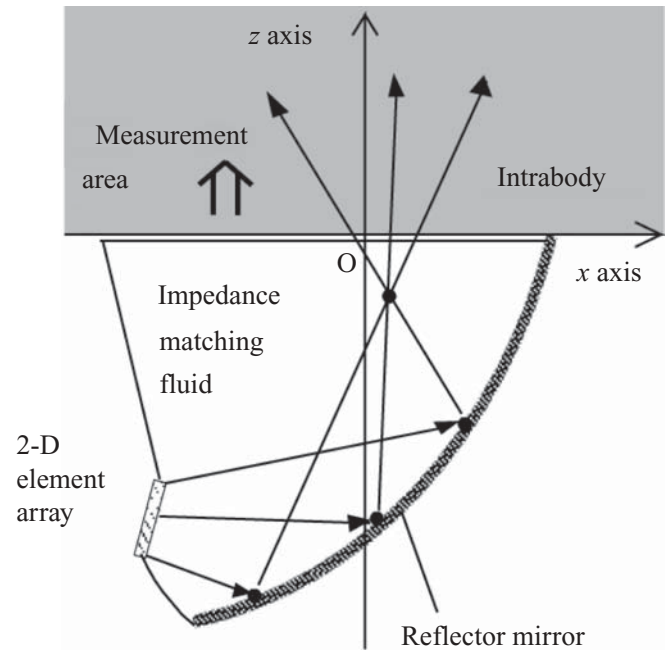


Fig. 1. Schematic of the system in the transmit phase. O is the origin of the coordinate system. 2-D, two-dimensional

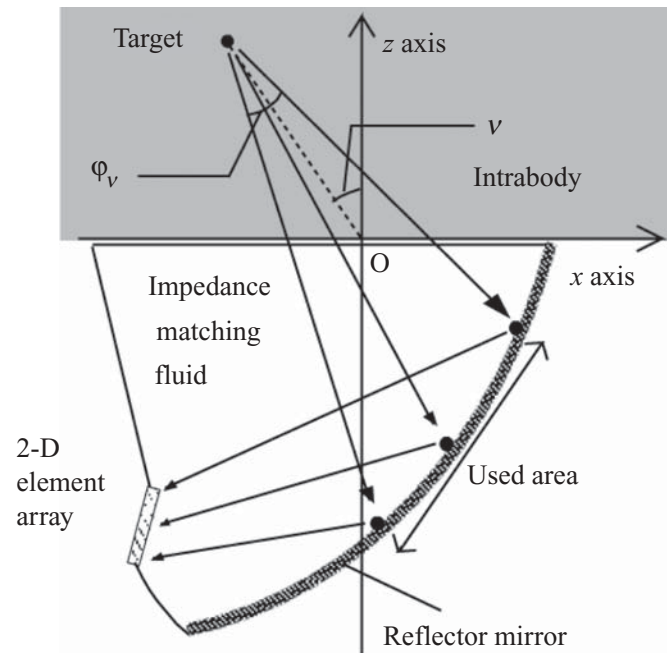


Fig. 2. Schematic of the system in the receive phase

event, which enables real-time 3-D imaging. Assuming that the propagation velocity of sound is 1600 m/s, if the maximum measuring range is 0.16 m, it is theoretically possible to realize a frame rate of 5000 3-D images/s if the SNR is sufficiently high.

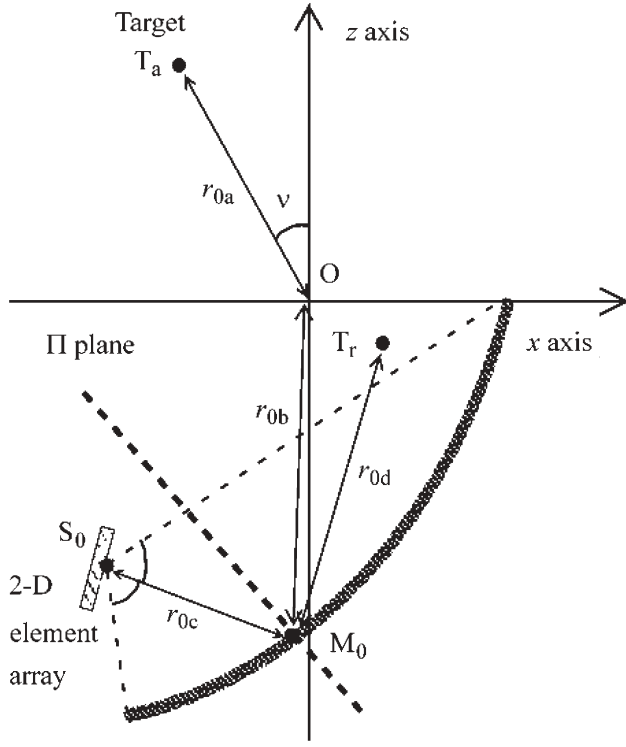


Fig. 4. Schematic of the mirror and array configuration for calculations in the time domain

$$\begin{aligned}
 P_{S_1}(t) &\cong P_{1S_1}(t) * F^{-1}[p_{2S_1}(\omega)] \\
 &= \sum P_{1S_1} \{ t - (r_{1a} + r_{1b} + r_{2a} + r_{2b} + r_3) / c_0 \} \\
 &\quad \left\{ \frac{\Delta c}{c_0} + (1 + \cos \theta_1) \frac{\Delta \rho}{2\rho_0} \right\} \frac{\mathbf{r}_{2a} \cdot \mathbf{n}_M}{r_{2a} n_M} \frac{\Delta S}{(r_{1a} + r_{1b})(r_{2a} + r_{2b}) r_3}
 \end{aligned} \quad (13)$$

$$P_{1S_1}(t) = F^{-1}[p_{1S_1}(\omega)] \quad (14)$$

The received signal on the element at S_1 , $P_{S_1}(t)'$, is proportional to $P_{S_1}(t)$.

Image reconstruction

We reconstructed the images of targets from the distributed images on the array by numerical back projection. In a similar approach to the calculation of the received signal, we define an element and the measurement point located at S_{2m} and T_b , respectively, as shown in Fig. 5. Assuming that the received signal is proportional to the estimated volume velocity at S_{2m} , the estimated velocity potential at M is given by:

$$\Phi_M(\omega)' \propto \sum_m \frac{p_m(\omega)' e^{-(jk+\alpha_1)r_3}^*}{2\pi r_3'} \quad (15)$$

$$p_m(\omega)' = F^{-1}[P_{S_m}(t)'] \quad (16)$$

where $\mathbf{r}_3' = \overline{S_{2m}M}$, $r_3' = |\mathbf{r}_3'|$, $P_{S_m}(t)'$ is the received signal on the element at S_m in the time domain, and $p_m(\omega)'^*$ is the

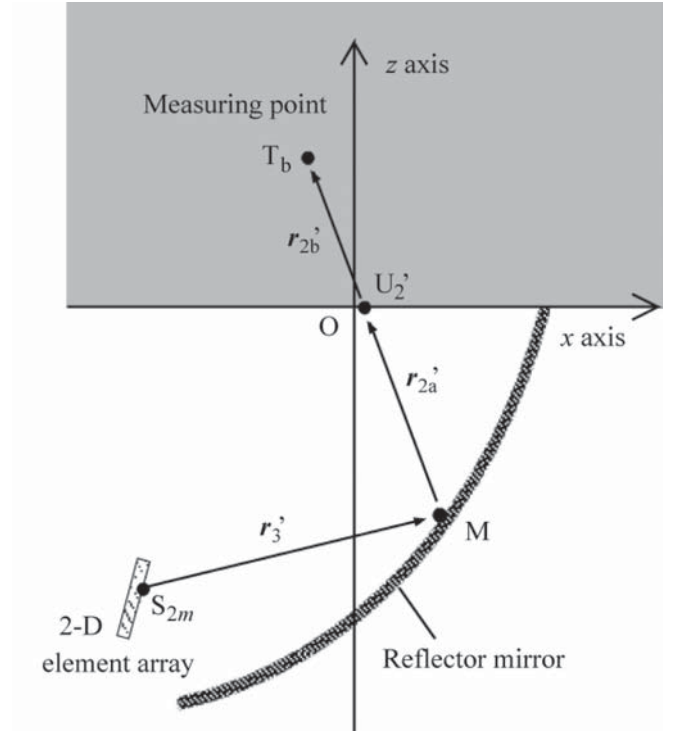


Fig. 5. Arrangement of a 2-D element array and mirror for numerical back projection

complex conjugate of $p_m(\omega)'$. The estimated volume velocity at M is given by:

$$V_M' = - \frac{\partial \Phi_M(\omega)'}{\partial r_3'} \frac{\mathbf{r}_3' \cdot \mathbf{n}_M}{r_3' n_M} \Delta S \quad (17)$$

The estimated velocity potential and the estimated pressure variation at T_b are given by:

$$\Phi_{T_b}(\omega)' = \int_S V_M' \frac{e^{-(jk+\alpha_1)r_{2a}' - (jk+\alpha_2)r_{2b}'}}{2\pi(r_{2a}' + r_{2b}')^2} dS \quad (18)$$

$$\begin{aligned}
 p_{T_b}(\omega)' &= j\rho\omega\Phi_{T_b}(\omega)' \\
 &\propto \int_S \sum_m \frac{-k^2 p_m(\omega)' e^{-(jk+\alpha_1)(r_{2a}'+r_3') - (jk+\alpha_2)r_{2b}'}}{4\pi^2(r_{2a}' + r_{2b}')^2 r_3'} \frac{\mathbf{r}_3' \cdot \mathbf{n}_M}{r_3' n_M} dS
 \end{aligned} \quad (19)$$

respectively, where $\mathbf{r}_{2a}' = \overline{MU_2'}$, $\mathbf{r}_{2v}' = \overline{U_2'T_b}$, $r_{2a}' = |\mathbf{r}_{2a}'|$, and $r_{2b}' = |\mathbf{r}_{2b}'|$.

The pressure variation in the time domain at T_b is given by the inverse Fourier transformation of $p_{T_b}(\omega)'$ as:

$$P_{T_b}(t)' = F^{-1}[p_{T_b}(\omega)'] \quad (20)$$

We also introduce an assumption:

$$e^{-\alpha_1(r_{2a}'+r_3') - \alpha_2 r_{2b}'} \cong e^{-\alpha_1(r_{0b}+r_{0c}) - \alpha_2 r_{0a}} \quad (21)$$

Later, we evaluate the validity of this assumption also. By introducing this assumption, the following equations are obtained from Eq. 19:

$$p_{T_b}(\omega)' \propto \sum_m p_{1T_b}(\omega)' p_{2T_b}(\omega)' \quad (22)$$

$$P_{1T_b}(\omega)' = -k^2 e^{-\alpha_1(r_{0b}+r_{0c})-\alpha_2 r_{0a}} p_m(\omega)' / (4\pi^2) \quad (23)$$

$$P_{2T_b}(\omega)' = \int_S \frac{e^{-jk(r_{2a}'+r_{2b}'+r_3')}}{(r_{2a}'+r_{2b}')r_3' r_3' n_M} \mathbf{r}_3' \cdot \mathbf{n}_M dS \quad (24)$$

In the same way as for Eqs. 13 and 14, the following equations are obtained:

$$\begin{aligned} P_{T_b}(t)' &\propto \sum_m P_{1T_b}(t)' * F^{-1} [P_{2T_b}(\omega)'] \\ &= \sum_m P_{1T_b} \left\{ t - \left(r_{1a}' + r_{2b}' + r_3' \right) / c_0 \right\} \frac{\mathbf{r}_3' \cdot \mathbf{n}_M}{r_3' n_M} \frac{\Delta S}{(r_{2a}' + r_{2b}') r_3'} \end{aligned} \quad (25)$$

$$P_{1T_b}(t)' = F^{-1} [P_{1T_b}(\omega)'] \quad (26)$$

The estimated power at T_b , the objective function, is given by:

$$W_{T_b}(t)' \propto P_{T_b}(t)' P_{T_b}(t)'^* \quad (27)$$

When an ultrasound wave radiating from a point source is measured at a surface and the phase is reversed, the reversed wave projected backward from the surface is focused at the radiation point. Therefore, these functions are sufficient for 3-D image construction.

Calculation parameters

To investigate the spatial resolution of the proposed method, we set the parameters as follows: mean propagation velocity $c_0 = 1600$ m/s, density of the undisturbed medium $\rho_0 = 1.08 \times 10^3$ kg/m³, the variation of the propagation velocity $\Delta c = -300$ m/s, and the variation of the density $\Delta \rho = -1.0 \times 10^2$ kg/m³. The attenuation coefficients α_1 and α_2 were $2.0(\omega/2\pi)^2 \times 10^{-14}$ and $5.0(\omega/2\pi) \times 10^{-6}$ Np/m, respectively. In this method, as in the digital beamforming method, the element pitch is 0.5λ to prevent grating lobes, where $\lambda = c/f_0$ is the wavelength at the center frequency. Therefore, the radiating high-frequency ultrasound requires miniaturization of the element size. In this article, we set the element pitch at 5×10^{-4} m. This means that $\lambda = 0.001$ m, i.e., the center frequency $f_0 = 1.6$ MHz. Since the cost is proportional to the number of elements on the array, to employ a large array is unrealistic. Many researchers have investigated 2-D arrays with 500–1000 elements.^{13,14} We employed a circular array 0.016 m in diameter with 797 elements, as shown in Fig. 6.

Figure 7 shows the broadband pulse transmitted by the elements in this array, where the -6 dB fractional bandwidth is 60%. The spectrum of the pulse is expressed as:

$$S(\omega) = A_c \omega^2 e^{-B_c(\omega-\mu)^2} \quad (28)$$

where A_c and B_c are coefficients and μ is the central angular frequency. Because we proposed that a wide transmit beam with high acoustic power can be synthesized using a focusing method,¹⁹ we assumed that the synthesized transmit beam is an omnidirectional spherical wave whose spectrum is proportional to $S(\omega)e^{-\alpha_1(r_{0c}+r_{0d})}$, where $r_{0d} = |\mathbf{M}_0 \mathbf{T}_1|$ and $e^{-\alpha_1(r_{0c}+r_{0d})}$ is caused by the attenuation through the impedance-matching fluid.

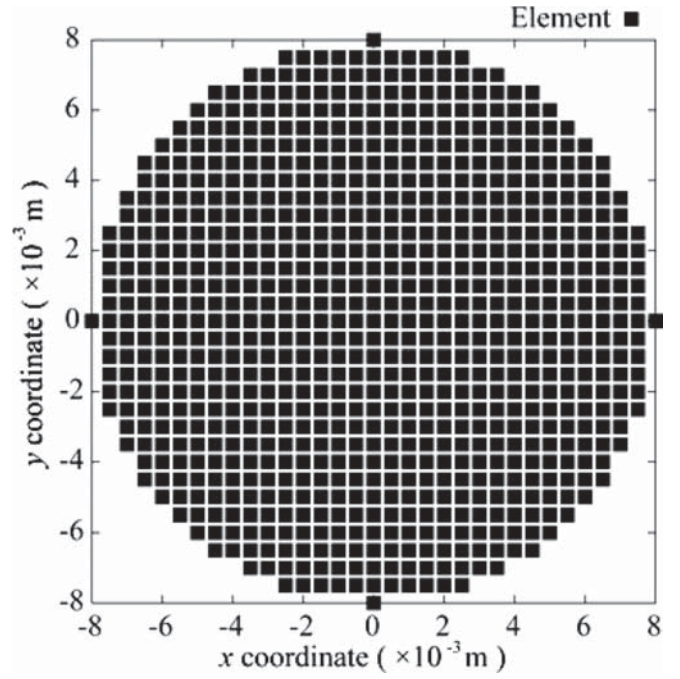


Fig. 6. Element pattern for a 797-element array

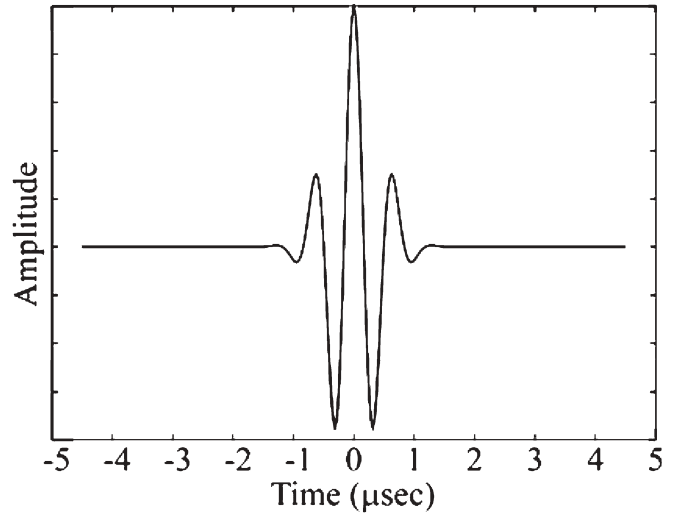


Fig. 7. Waveform of the pulse used in this research

Optimization of the reflector shape and the array configuration

Because we reconstruct the received signal by numerical back projection, there is no need to focus it on the array. This indicates that a reflector shape suitable for this method may be different from traditional shapes. Utilizing geometric optics, we optimized the reflector shape and the array configuration for a wide measurement area with high spatial resolution.

Figure 2 schematically shows the ray trace of an echo in geometric optics. Part of the echo reflected on the mirror is received on the array. We call the reflected region on the

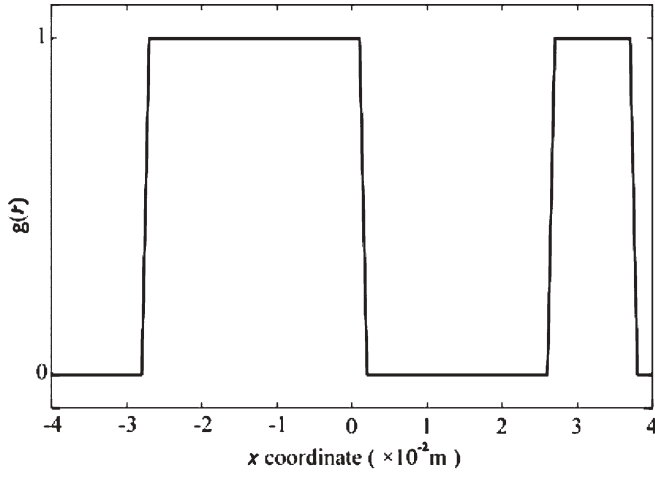


Fig. 8. The area of the mirror used in the x - z plane. The value of the used area is 1 and that of the area not used is 0. The x , y , and z coordinates of the target were 0.005, 0, and 0.07 m, respectively

mirror the used area, and define φ_v as the visual angle of the used area from the target position as follows:

$$\begin{aligned}\varphi_v &= \int_S \frac{g(\mathbf{r})}{r^3} \mathbf{r} \cdot d\mathbf{S} \\ &= \sum g(\mathbf{r}) \frac{\mathbf{r} \cdot \mathbf{n}_M}{r^3 n_M} \Delta S \\ g(\mathbf{r}) &= \begin{cases} 1 & \text{if the point M is on the used area} \\ 0 & \text{else} \end{cases}\end{aligned}\quad (29)$$

$$(30)$$

where $\mathbf{r} = \mathbf{r}_{2a} + \mathbf{r}_{2b}$, $r = |\mathbf{r}|$, and v is the target direction from the z axis, as shown in Fig. 4.

First, when the used area consists of multiple groups, the sidelobe level is high because the main lobe is divided. Below, we investigate an example of such a case. Figure 8 shows the used area on the mirror in the x - z plane. The x , y , and z coordinates of the target are 0.005, 0, and 0.07 m, respectively. A function value of 1 means that the region of the mirror is a used area, and 0 means that it is an unused area. In this case, the echo reflected on a region whose x coordinate is greater than 0.002 m and less than 0.026 m is not received on the array. Thus, the used area consists of two groups: the region on the mirror whose x coordinate is negative and the right edge. Figure 9 shows the lateral resolution of this mirror for a depth of 0.07 m. The first sidelobe level is -5.9 dB, which would hinder medical diagnosis. Therefore, we discarded mirrors with a used area in the x - z plane or Π plane that consisted of multiple groups. The Π plane is perpendicular to both the x - z plane and the mirror, as shown in Fig. 4. The intersection of the Π plane and the mirror in the x - z plane is at the center in the visual angle of the mirror.

Next, we optimized the mirror shape under the above conditions. To realize sufficient lateral resolution and SNR using a small array, the echo should be gathered on the array. This means that the visual angle should be maximized. We set the evaluation function as:

$$E = E_X + E_Y \quad (31)$$

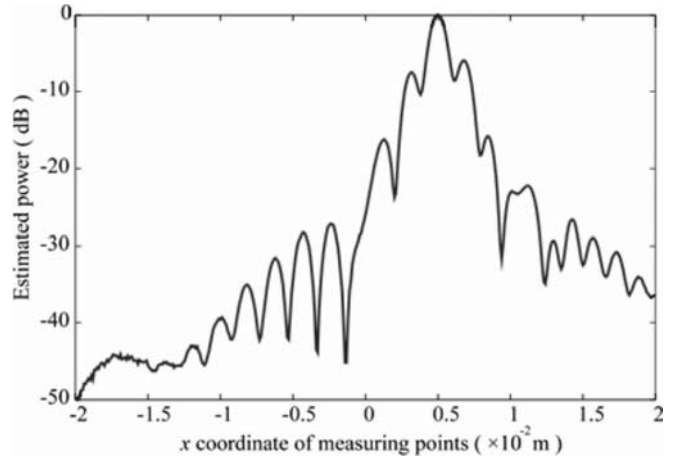


Fig. 9. Lateral resolution where the used area consists of multiple groups. The main lobe is divided, and thus the sidelobe level becomes high

$$E_X = \int_{v_{Xmin}}^{v_{Xmax}} \varphi_v dv = \sum_x \varphi_v \Delta v \quad (32)$$

$$E_Y = \int_{v_{Ymin}}^{v_{Ymax}} \varphi_v dv = \sum_y \varphi_v \Delta v \quad (33)$$

where E_X and E_Y are used when targets are in the x - z and y - z planes, respectively. As shown in Eq. 29, φ_v is determined indirectly by the shape of the reflecting mirror. Thus, the maximization of E becomes a problem of finding the optimum shape function of a mirror that gives the highest value of E .

We call the shape functions of the optimized reflector in the x - z and Π planes f_x and f_y , respectively. These functions are given by:

$$f_x = l_{1x} \left[\frac{1 - \cos(l_{3x}x + l_{3x}x_{max} + l_{4x})}{1 - \cos(l_{4x})} \right]^{l_{2x}} - \frac{1 - \cos(l_{4x})}{1 - \cos(2l_{3x}x_{max} + l_{4x})} \left[\frac{1 - \cos(l_{4x})}{1 - \cos(l_{4x})} \right]^{l_{2x}} \quad (34)$$

$$f_y = l_{1y} \left\{ 1 - \cos(l_{3y}y) \right\}^{l_{2y}} / \left\{ 1 - \cos(l_{3y}y_{max}) \right\}^{l_{2y}} \quad (35)$$

where x_{max} and y_{max} are half of the mirror width in the x - z and Π planes, respectively. They are in fact the heights from the bottom points of the reflector in each plane.

Since we determined the visual angle of the measurement area as $\pi/3$, we set $v_{Xmax} = v_{Ymax} = \pi/6$ and $v_{Xmin} = v_{Ymin} = -\pi/6$. Then, we optimize l_{1x} , l_{2x} , l_{3x} , l_{4x} , l_{1y} , l_{2y} , l_{3y} , x_{max} , and y_{max} by maximizing the evaluation function, E . The range of each variable is as follows: $0.025 \text{ m} \leq x_{max} \leq 0.04 \text{ m}$, $0.025 \text{ m} \leq y_{max} \leq 0.04 \text{ m}$, $0.01 \text{ m} \leq l_{1x} \leq 0.1 \text{ m}$, $0.5 \leq l_{2x} \leq 3$, $\pi/40 \leq l_{3x}x_{max}$, $0 \leq l_{4x}$, $2l_{3x}x_{max} + l_{4x} \leq \pi/2$, $0.01 \text{ m} \leq l_{1y} \leq 0.1 \text{ m}$, $0.5 \leq l_{2y} \leq 3$, and $\pi/20 \leq l_{3y}y_{max} \leq \pi/2$.

It is thought that many local maximums of E exist. We first optimized f_x and f_y by maximizing E_X and E_Y , respectively, which is a 2-D problem. We then set this as the initial value of the mirror shape, and optimized by maximizing E , which is a 3-D problem. The variables of the optimized reflector mirror were $x_{max} = 0.031 \text{ m}$, $y_{max} = 0.04 \text{ m}$, $l_{1x} = 0.06 \text{ m}$, $l_{2x} = 2.3$, $l_{3x} = \pi/124$, $l_{4x} = \pi/20$, $l_{1y} = 0.015 \text{ m}$, $l_{2y} = 1.4$, and $l_{3y} = 3\pi/160$.

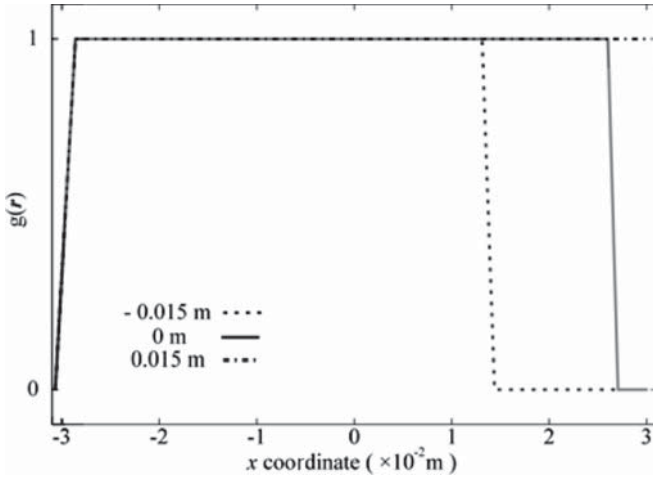


Fig. 10. The used area on the optimized mirror in the x - z plane. The value of the used area is 1 and that of the area not used is 0. The x coordinates of targets are -0.015 , 0 , and 0.015 m. The target range is 0.07 m in the x - z plane

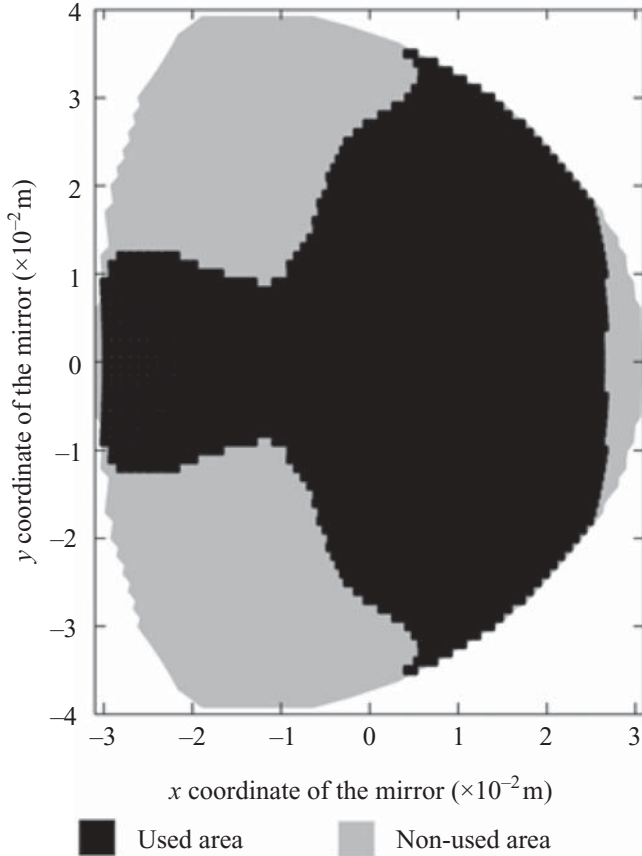


Fig. 11. The used area on a mirror projected onto the x - y plane when the target is at the center at a depth of 0.07 m

Figure 10 shows the used area of the optimized mirror in the x - z plane. The x coordinates of the targets were -0.015 , 0 , and 0.015 m. The target range was 0.07 m. Figure 11 shows the used area projected onto the x - y plane for a central target at a depth of 0.07 m.

Since a large part of the echo reflected by the mirror returns to the array, the visual angle of the used area from the target, A_H , is larger than that of an array of the same size put at the center of the x - y plane, A_{DBF} . We call the ratio of A_H to A_{DBF} the receive efficiency, R_H :

$$R_H = A_H / A_{\text{DBF}} \quad (36)$$

The echo reflected by the used area is received on the array; thus, R_H is closely related to the SNR improvement of the proposed method compared to that of a digital beamforming method with an array of the same size.²⁰ For example, for a central target at a depth of 0.07 m, R_H is 6.2 . In this case, the SNR improvement of the proposed method compared with a digital beamforming method is 7.8 dB, as shown in the Discussion section. Henceforth, we normalize the estimated power of the image at each measuring point to make the peak power R_H when we calculate the lateral resolution of the proposed imager.

Sidelobe suppression in image reconstruction

For medical diagnoses, we need to decrease the sidelobe levels of the proposed imager. In the proposed method, echoes reflected on the mirror only are received on the array. Breaks in the received signal occur at the edge of the mirror and result in a high sidelobe level. The reflection ratio of the mirror should taper off toward the edge, but in practice it is difficult to make such a mirror. Therefore, we employ a tapered reflection ratio for the mirror during image reconstruction from the signal received on the array. Since images are reconstructed from received signals by numerical back projection, the reflection ratio of the mirror can be set freely during image reconstruction. We will now investigate the effect of tapering the reflection ratio of the mirror.

The used area on the reflector depends on the target position. Therefore, weighting the reflection ratio of the mirror is useful to reduce the sidelobe level at the cost of some loss of SNR and lateral resolution. Because of the reflection ratio tapering off, Eqs. 18 and 25 are changed as follows:

$$\Phi_{T_b}(\omega)' = \int_S a_M V_M' \frac{e^{-(jk+\alpha_1)r_{2a}' - (jk+\alpha_2)r_{2b}'}}{2\pi(r_{2a}' + r_{2b}')} dS \quad (37)$$

$$P_{T_b}(t)' = \sum P_{1T_b} \left\{ t - (r_{1a}' + r_{2b}' + r_3') / c_0 \right\} \frac{r_3' \cdot \mathbf{n}_M}{r_3' n_M} \frac{a_M \Delta S}{(r_{2a}' + r_{2b}') r_3'} \quad (38)$$

where a_M^2 is the reflection ratio of the mirror at point M in the numerical back projection.

The first sidelobe level of a digital beamforming imager with a dense circular 2-D array is -18.3 dB. Therefore, we set the threshold at -18.3 dB. If the sidelobe level of a measuring direction is higher than the threshold, we use this method to decrease the sidelobe level to less than the threshold.

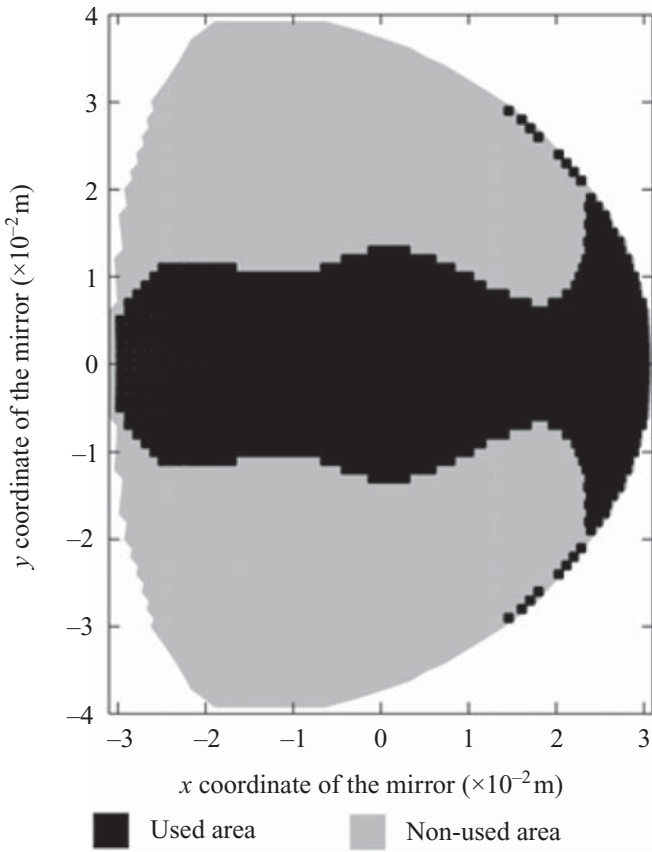


Fig. 12. The used area on a mirror projected onto the x - y plane when the x coordinate of the target is 0.015 m in the x - z plane at a depth of 0.07 m

For a depth of 0.07 m in the x - z plane, the first sidelobe level is highest when the x coordinate of the target is 0.015 m. Figure 12 shows the used area on an optimized reflector in such a case. A break occurs in the received signal at the right edge of the mirror; thus, we set the reflection ratio of the mirror to taper off at the right edge, as shown in Fig. 13. The visual angle decrease of the used area from the target is -0.18 dB. This means that tapering results in a slight decrease in the estimated power. Figure 14 shows the lateral resolution of the proposed method with and without tapering. The sidelobe level is suppressed to less than -21 dB at the cost of a slight deterioration in the SNR and lateral resolution.

Results

In this section, we examine the spatial resolution of the proposed imager. First, we compared the spatial resolution of a phased-array imager with a linear array to that of the proposed imager. When using a linear or convex array for 3-D imaging, the receive beams can be dynamically focused in the plane parallel to the longitudinal axis of the array. In contrast, in the perpendicular plane, transmit and receive beams are focused by acoustic lenses. This means that the focal distance is fixed. Figure 15 shows the spatial resolution

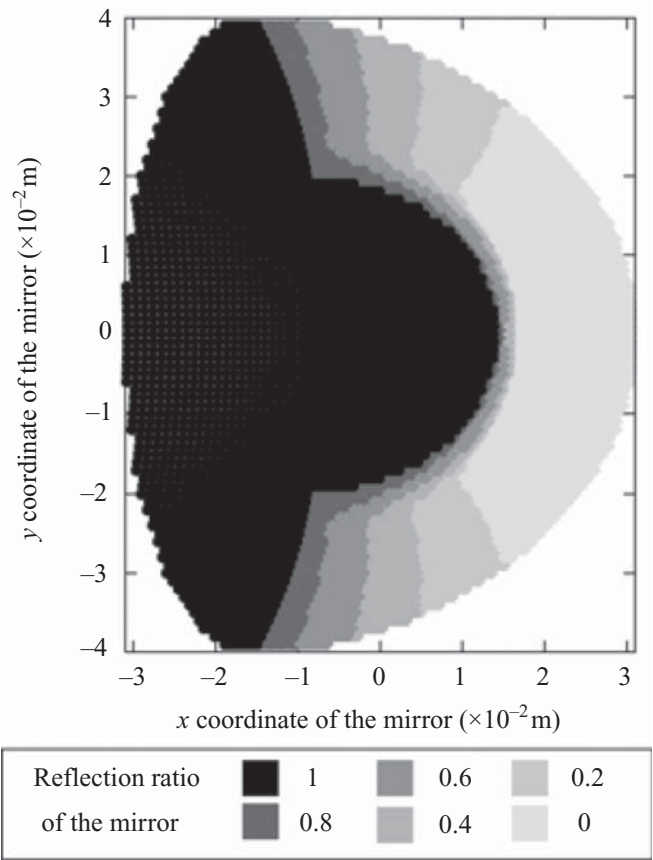


Fig. 13. The taper function for the reflection ratio on the mirror used for numerical back projection

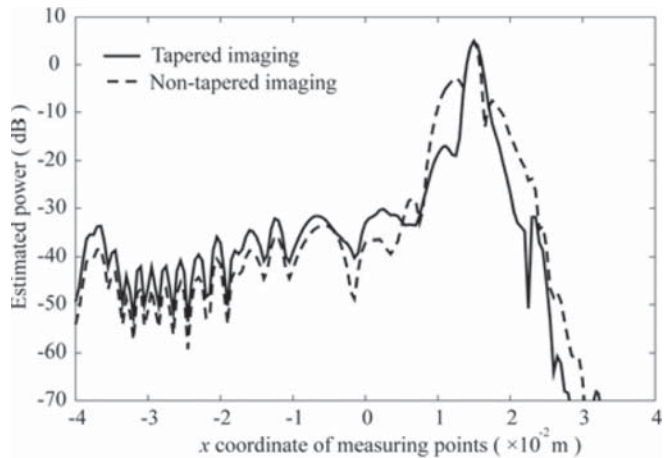


Fig. 14. Lateral resolution of a tapered and nontapered proposed imager with an array 0.016 m wide in a 3-D problem. The x coordinate of the target is 0.015 m, and those of the measuring points are from -0.04 to 0.04 m

of a phased-array imager in a perpendicular plane when the array width is 0.016 m and the focal length is 0.07 m. The target is at the center at depths of 0.02 and 0.07 m. If targets are near the focal zone, the spatial resolution is high, but spurious images of high amplitude appear over a wide area when the distance between the focal zone and the target is

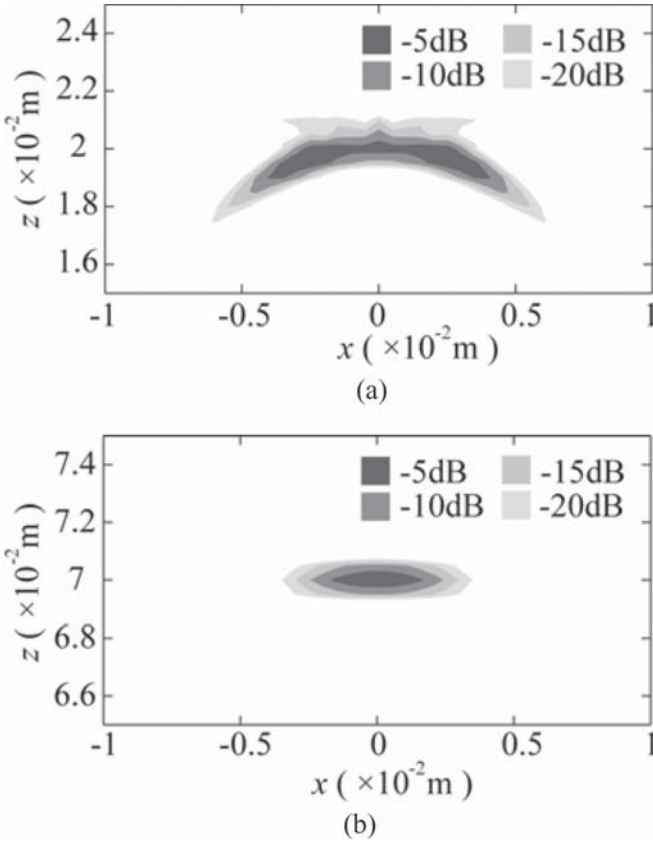


Fig. 15. Spatial resolution of a phased-array imager with a 1-D array. The focal length of the acoustic lenses is 0.07 m and the target is at the center at depths of 0.02 m (a) and 0.07 m (b). This plane is perpendicular to the longitudinal axis of the linear array

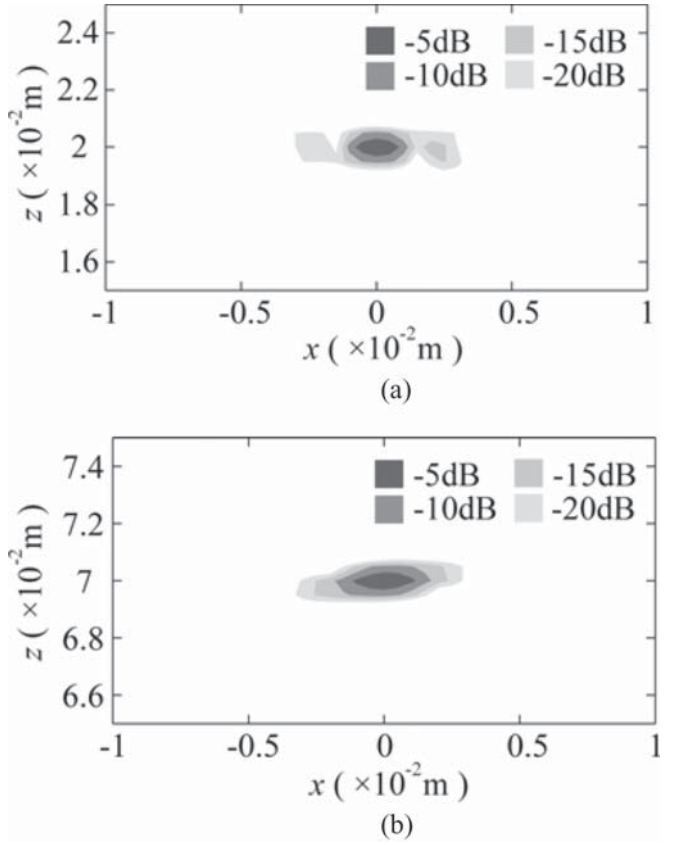


Fig. 16. Spatial resolution of the proposed imager in the x - z plane. Targets were located at the center at depths of 0.02 m (a) and 0.07 m (b)

large, as shown in this figure. This significantly hampers medical diagnoses.

Figure 16 shows the spatial resolution of the proposed method when the optimized reflector mirror is used. The target ranges are 0.02 and 0.07 m. In this method, receive beams are dynamically focused to all measurement points and good spatial resolution can be acquired.

Figure 17 shows the lateral resolution of the proposed imager with a 0.016 m wide array at a range of 0.07 m in the x - z and y - z planes. The x coordinates of targets in the x - z plane are -0.03 , -0.015 , 0 , 0.015 , and 0.03 m, and the y coordinates in the y - z plane are 0 , 0.015 , and 0.03 m. Sidelobe levels in all these examples are less than -21 dB.

To evaluate the validity of the assumptions made in Eqs. 9 and 21, we calculated the estimated power without these assumptions. The calculation in the frequency domain utilizing Eqs. 8 and 20 entails a high computational cost, and thus we calculated the estimated power at two measurement points. These points were at $y = 0$ and 0.004 m in the y - z plane for a 0.07 m depth when a point target is located at the center at a 0.07 m depth, i.e., we compared two measurement points in Fig. 17b when a point target was placed at the center. The differences between a values calculated with and without the assumptions in terms of attenuation at the measurement points $y = 0$ and 0.004 m are 0.216 dB

and 0.208 dB, respectively. This indicates that the assumptions of Eqs. 9 and 21 are valid.

The lateral resolution for $y = 0.015$ m in the y - z plane has swells at $y = 0.013$ and 0.017 m. These are created by the small used area separated from the main used area, as shown in Fig. 18. When images are reconstructed using a taper function to remove the small used area, -3 dB lateral resolution deteriorates slightly and the swells vanish.

Discussion

Evaluation of the radiation pattern

In this section, we compare the spatial resolution of the proposed imaging scheme with that of the digital beamforming method. The x - z and y - z plane -3 dB lateral resolutions at the center for a depth of 0.07 m are about 1.70λ and 1.41λ , respectively, which is the same as that of a digital beamforming imager with an elliptic array 0.041 m long and 0.051 m wide, as shown in Fig. 19. Because the elements are spaced at intervals of one-half of a wavelength on the array, the area of the array is proportional to the number of elements. Therefore, the number of elements can be reduced

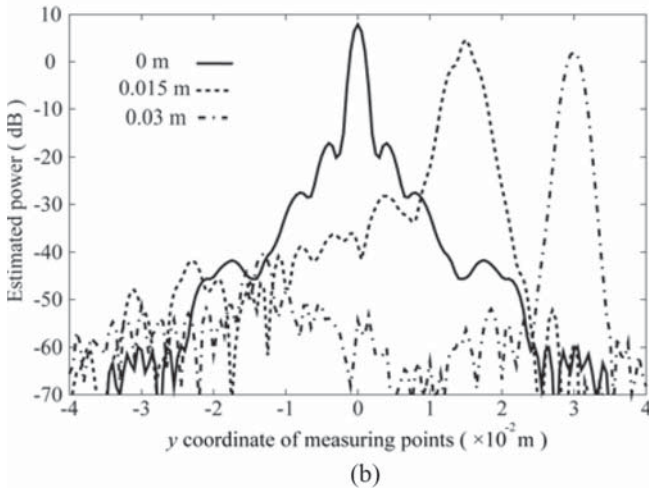
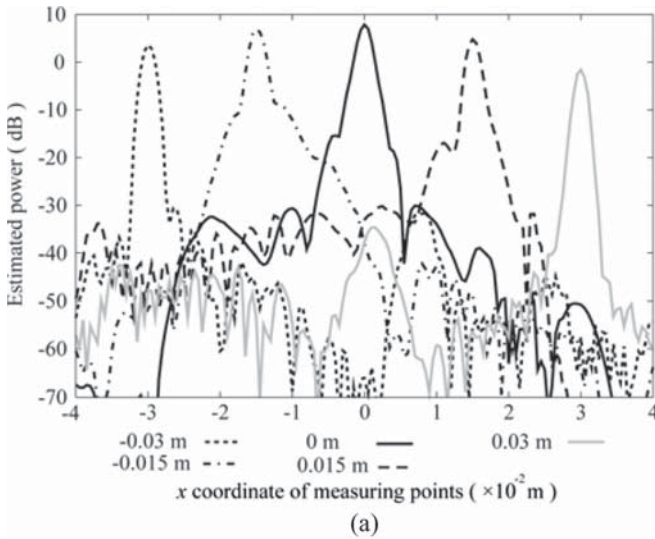


Fig. 17. Lateral resolution of the proposed imager with an array 0.016 m wide in the x - z (a) and y - z planes (b) for a depth of 0.07 m. a The x coordinates of targets were -0.03 , -0.015 , 0 , 0.015 , and 0.03 m. b The y coordinates of targets were 0 , 0.015 , and 0.03 m

to about $1/8.2$ that of a dense 2-D array having the same spatial resolution.

Consideration of the signal-to-noise ratio

A common problem for a digital beamforming imager is the low signal-to-noise ratio due to the wide transmit beam. Since this proposed method also uses wide transmit beams, we need to investigate the SNR with this method. In this section, we compare the SNR of a phased array, digital beamforming, and the proposed method.

Noise in an acoustic image is primarily determined by uncorrelated electronic noise in the receiver. For this discussion we follow the investigation of Karaman et al.¹⁵ For a phased-array imager, all transmit pulses are focused and the signal power is proportional to N_t^2 at the focal region, where N_t is the number of transmit elements. Assuming uncorrelated noise, a multi-element receiver causes a SNR

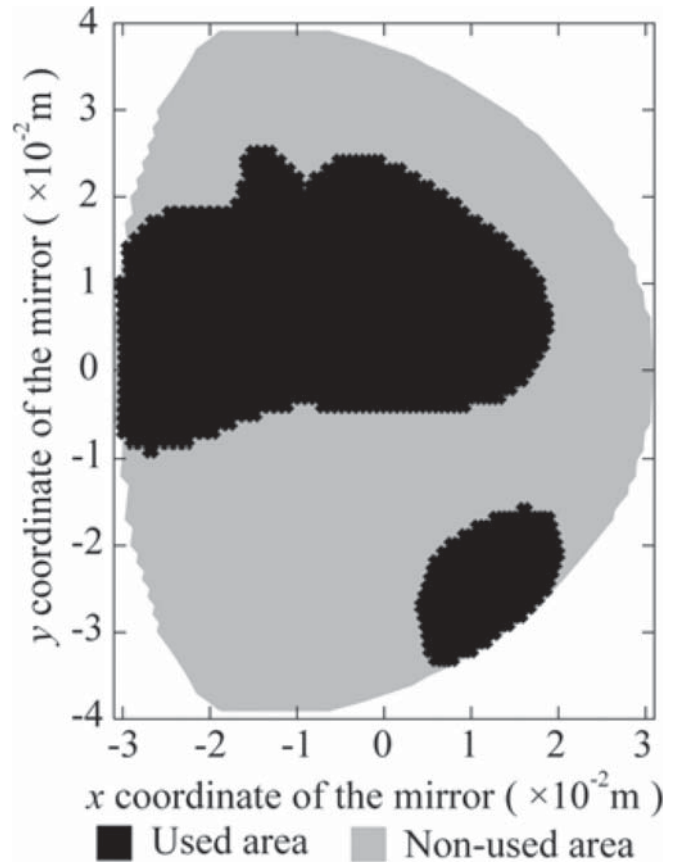


Fig. 18. The used area on a mirror projected onto the x - y plane where the y coordinate of the target was 0.015 m in the y - z plane at a depth of 0.07 m

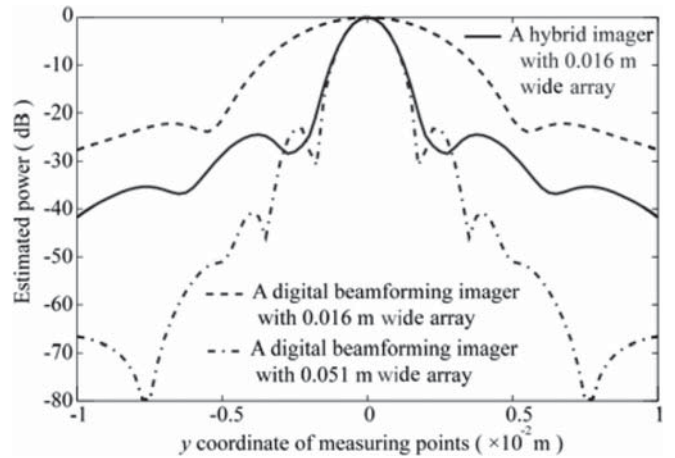


Fig. 19. Lateral resolution of the proposed imager with an array 0.016 m wide and digital beamforming imagers with arrays 0.016 m and 0.051 m wide. The target was at the center at a depth of 0.07 m

improvement of $10 \log(N_r)$ dB, where N_r is the number of receive elements. Consequently, the SNR of a phased-array imager, SNR_{PA} , satisfies the following equation:

$$\text{SNR}_{\text{PA}}/\text{SNR}_0 = 10 \log(N_t^2 N_r) \quad (39)$$

where SNR_0 is the SNR of a single-element imager.

For a digital beamforming imager, a defocused multi-element transmitter synthesizes single-element spatial resolution, and the signal power is N_t times that of a single-element transmitter. Consequently, the SNR of a synthetic aperture imager, SNR_{DBF} , satisfies the following equation:

$$\text{SNR}_{\text{DBF}}/\text{SNR}_0 = 10 \log(N_t N_r N_c) \quad (40)$$

where N_c is the number of coherently integrated pulses.

For the proposed imager, a multi-element transmitter with proper time delay synthesizes a single-element spatial response, similar to a digital beamforming imager with defocusing, and it is expected that the signal power will be N_t times as intensive as that of a single element transmitter. R_H is the SNR improvement of the proposed method compared with the digital beamforming method. Because a large part of the echo reflected by the mirror returns to the array, R_H is usually larger than 1. We further define P_{Hl} , P_l , and b_l , satisfying the following expression:

$$P_{Hl} = \sqrt{R_H b_l} P_l D_t D_r \quad (41)$$

where P_{Hl} is the received signal amplitude in the proposed method, P_l is that in the digital beamforming method, and b_l is a coefficient. D_t and D_r are caused by the attenuation through the impedance-matching fluid in the transmit and receive phases. Since the power summation of received signals is proportional to the power of the returned echoes, the following expressions are given:

$$W_H \propto \sum_l P_{Hl}^2 = R_H \sum_l (b_l P_l^2) D_t^2 D_r^2 \quad (42)$$

$$W_{\text{DBF}} \propto \sum_l P_l^2 \quad (43)$$

The coefficient b_l satisfies the following equation:

$$\sum_l (b_l P_l^2) = \sum_l P_l^2 \quad (44)$$

Because of reconstruction based on numerical back projection, the estimated signal amplitude, S_{HA} , is given by:

$$S_{\text{HA}} \propto \sum_l (\sqrt{R_H b_l} P_{Hl}) e^{-2\alpha_1(r_{0a} + r_{0b})} \quad (45)$$

where we introduce the approximation that $D_t = D_r = e^{-\alpha_1(r_{0a} + r_{0b})}$.

The estimated signal power, S_{HP} , satisfies the following equation:

$$S_{\text{HP}} \propto R_H^2 \left(\sum_l P_l \right)^2 e^{-4\alpha_1(r_{0a} + r_{0b})} \quad (46)$$

Assuming uncorrelated noise, the SNR of the proposed imager, SNR_H , is given by the relation:

$$\text{SNR}_H/\text{SNR}_0 = 10 \log(N_t N_r R_H N_c e^{-4\alpha_1(r_{0a} + r_{0b})}) \quad (47)$$

For example, with an 800-element array ($N_t = N_r = 800$), with water as the impedance-matching fluid [$\alpha_1 = 2.0(\omega/2\pi)^2 \times 10^{-14}$ Np/m], $r_{0a} + r_{0b} = 0.085$ m; if the receive efficiency, R_H , is 6.2, and the number of coherently integrated pulses, N_c , is 260, the proposed imager realizes the following SNR:

$$\text{SNR}_H/\text{SNR}_{\text{SA}} = 7.8 \text{ [dB]} \quad (48)$$

$$\text{SNR}_H/\text{SNR}_{\text{PA}} = 3.0 \text{ [dB]} \quad (49)$$

In this case, 3-D images can be acquired at a rate of 19 images/s. When the impedance-matching fluid is ultrasound jelly, the SNR improvements are 6.7 and 1.9 dB, respectively.

For cardiology, higher time resolution is needed. Assuming a heart rate of 80 beats/min and the distance moved in a beat cycle to be 0.02 m, the maximum speed is about 0.04 m/s. To improve the SNR, we can use coherent integration when the target moves 1/4 of a wavelength. When that wavelength is 0.001 m, the maximum coherent integration time is 1/160 second, i.e., $N_c = 30$. This means that more than 160 images/s are needed to measure the heart when the wavelength is less than 0.001 m. The proposed scheme is suited for such purposes.

Conclusion

For a high-resolution acoustic real-time 3-D imaging system, we proposed a system based on a hybrid method with a reflector mirror and a small dense array. Utilizing this scheme, images of the whole measurement area can be reconstructed from a single transmit and receive event, thus enabling real-time 3-D imaging. Receiving a large part of the echo focused by the mirror has the same effect as using a large array. This method realizes lateral resolutions of 1.70λ in the x - z and 1.41λ in the y - z planes at a depth of 0.07 m, when the center frequency is 1.6 MHz, the reflector is 0.062 m long and 0.08 m wide, and the array is a circle 0.016 m in diameter. This shows that the number of elements can be reduced to about 1/8.2 that of a dense 2-D array having the same spatial resolution but using a digital beamforming method. Because we make the reflection ratio of the mirror taper off in the numerical back projection, the sidelobe level is suppressed to less than -21 dB. The maximum theoretical frame rate is 5000 frames/s when the SNR is sufficiently high. Since the transmit beam is synthesized by all elements in the array, a sufficiently high SNR is achieved. In cases where the frame rate is 19 images/s, the SNR improvements compared to the conventional phased array method and the digital beamforming method with defocusing are 3.0 dB and 7.8 dB, respectively.

References

- Shoup TA, Hart J. Ultrasonic imaging systems. In: Proceedings of the IEEE Ultrasonics Symposium. IEEE: Piscataway, NJ, USA; Editor: McAvoy BR; 1988, p. 863–71.
- Nelson TR, Pretorius DH. Three-dimensional ultrasound imaging. *Ultrasound Med Biol* 1998;24:1243–70.
- Berg S, Torp H, Martens D, et al. Dynamic three-dimensional freehand echocardiography using raw digital ultrasound data. *Ultrasound Med Biol* 1999;25:745–53.
- Canals R, Lamarque G, Chatain P. Volumetric ultrasound system for left ventricle motion imaging. *IEEE Trans Ultrason Ferroelectr Freq Control* 1999;46:1527–38.
- Turnbull DH, Foster FS. Beam steering with pulsed two-dimensional transducer arrays. *IEEE Trans Ultrason Ferroelectr Freq Control* 1991;38:320–33.

6. Turnbull DH, Foster FS. Simulation of B-scan images from two-dimensional transducer arrays: Part 2 – Comparison between linear and two-dimensional phased arrays. *Ultrason Imaging* 1992;14:334–53.
7. Weber PK, Schmitt RM, Tylkowski BD, et al. Optimization of random sparse 2-D transducer arrays for 3-D electronic beam steering and focusing. In: *Proceedings of the IEEE Ultrasonics Symposium*. IEEE: Piscataway, NJ, USA; Editor: Levy M, McAvoy BR, and Schneider SC; 1994. p. 1503–6.
8. Holm S, Elgetun B, Dahl G. Weight- and layout-optimized sparse arrays. In: *Proceedings of the International Workshop on Sampling Theory and Applications*. University of Aveiro: Aveiro, Portugal; 1997. p. 97–102.
9. Schwartz JL, Steinberg BD. Ultrasparse ultrawideband arrays. *IEEE Trans Ultrason Ferroelectr Freq Control* 1998;45:376–93.
10. Sumanaweera TS, Schwartz J, Napolitano D. A spiral 2D phased array for 3D imaging. In: *Proceedings of IEEE Ultrasonics Symposium*. IEEE: Piscataway, NJ, USA; Editor: Levy M, McAvoy BR, and Schneider SC; 1999. p. 1271–74.
11. Smith SW, Pavey HG, Ramm OT. High-speed ultrasound volumetric imaging system – Part 1: Transducer design and beam steering. *IEEE Trans Ultrason Ferroelectr Freq Control* 1991;38:100–8.
12. Lockwood GR, Li P-C, O'Donnell M, et al. Optimizing the radiation pattern of sparse periodic linear arrays. *IEEE Trans Ultrason Ferroelectr Freq Control* 1996;43:7–14.
13. Lockwood GR, Foster FS. Optimizing the radiation pattern of sparse periodic two-dimensional arrays. *IEEE Trans Ultrason Ferroelectr Freq Control* 1996;43:15–9.
14. Austeng A, Holm S. Sparse 2-D arrays for 3-D phased array imaging – design methods. *IEEE Trans Ultrason Ferroelectr Freq Control* 2002;49:1073–86.
15. Karaman M, Li P-C, O'Donnell M. Synthetic aperture imaging for small-scale systems. *IEEE Trans Ultrason Ferroelectr Freq Control* 1995;42:429–42.
16. Lockwood GR, Talman JR, Brunke SS. Real-time 3-D ultrasound imaging using sparse synthetic aperture beamforming. *IEEE Trans Ultrason Ferroelectr Freq Control* 1998;45:980–8.
17. Bracewell RN. Numerical transforms. *Science* 1990;248:697–704.
18. Ueda M, Ichikawa H. Analysis of an echo signal reflected from a weakly scattering volume by a discrete model of the medium. *J Acoust Soc Am* 1981;70:1768–75.
19. Taki H, Sato T. A study on the radiation pattern using focusing method for a 3-D medical acoustic imaging system with a reflector and a 2-D array. In: *Proceedings of Symposium on Ultrasonic Electronics*. USE Program Committee: Shizuoka, Shizuoka, Japan: 2006, p. 149–50.
20. Taki H, Yashima H, Sato T. Study of the hybrid method and the sensor for a high-resolution ultrasound vision substitute system for the visually handicapped (in Japanese). *IEICE Trans Fundamentals* 2005;J88A:568–76.